

## What does mediated electrochemistry reveal about regional differences in the redox properties of Boom Clay?

Hoving, Alwina L.; Sander, Michael; Frederickx, Lander; Dugulan, Achim Iulian; Bruggeman, Christophe; Behrends, Thilo

**DOI**

[10.1016/j.apgeochem.2020.104681](https://doi.org/10.1016/j.apgeochem.2020.104681)

**Publication date**

2020

**Document Version**

Final published version

**Published in**

Applied Geochemistry

**Citation (APA)**

Hoving, A. L., Sander, M., Frederickx, L., Dugulan, A. I., Bruggeman, C., & Behrends, T. (2020). What does mediated electrochemistry reveal about regional differences in the redox properties of Boom Clay? *Applied Geochemistry*, 120, Article 104681. <https://doi.org/10.1016/j.apgeochem.2020.104681>

**Important note**

To cite this publication, please use the final published version (if applicable).  
Please check the document version above.

**Copyright**

Other than for strictly personal use, it is not permitted to download, forward or distribute the text or part of it, without the consent of the author(s) and/or copyright holder(s), unless the work is under an open content license such as Creative Commons.

**Takedown policy**

Please contact us and provide details if you believe this document breaches copyrights.  
We will remove access to the work immediately and investigate your claim.



## What does mediated electrochemistry reveal about regional differences in the redox properties of Boom Clay?

Alwina L. Hoving<sup>a,\*</sup>, Michael Sander<sup>b</sup>, Lander Frederickx<sup>c,e</sup>, Achim Iulian Dugulan<sup>d</sup>, Christophe Bruggeman<sup>c</sup>, Thilo Behrends<sup>a</sup>

<sup>a</sup> Department of Earth Sciences - Geochemistry, Faculty of Geosciences, Utrecht University, Princetonplein 9, 3584, CC, Utrecht, the Netherlands

<sup>b</sup> Institute of Biogeochemistry and Pollutant Dynamics (IBP), Department of Environmental Systems Science, ETH Zürich, 8092, Zürich, Switzerland

<sup>c</sup> Waste & Disposal Expert Group, Unit R&D Disposal, Belgian Nuclear Research Centre (SCK•CEN), Boeretang, 200, Mol, Belgium

<sup>d</sup> Fundamental Aspects of Materials and Energy Group, Delft University of Technology, Mekelweg 15, 2629, JB, Delft, the Netherlands

<sup>e</sup> Department of Earth and Environmental Sciences, KU Leuven, Celestijnenlaan 200E, 3001, Leuven, Belgium

### ARTICLE INFO

Editorial handling by Prof. M. Kersten

#### Keywords:

Mediated electrochemistry

Boom clay

Redox

Clay minerals

Pyrite

Natural organic matter

### ABSTRACT

The Boom Clay is a potential host rock for geological storage of radioactive waste in the Netherlands and Belgium. The redox properties of the host rock are important in the context of safety assessment as they affect the speciation and thus the mobility of redox sensitive radionuclides. In this study, redox properties of the clay were assessed by mediated electrochemical analyses. The electron donating (EDC) and accepting (EAC) capacities and reduction potential of a suite of Boom Clay samples were determined. Boom Clay samples from various locations in the Netherlands and Belgium were investigated in unaltered form, and after size separation or chemical treatment to relate variations in redox properties to regional differences in diagenetic history or in the assemblage of allogenic minerals. In the investigated samples, the EDC can be attributed to the oxidation of pyrite, Fe<sup>II</sup> in clay minerals and reduced natural organic matter (NOM) while the EAC can be ascribed to the reduction of Fe<sup>III</sup> in clay minerals and in Fe (oxyhydr)oxides. Combining Na-pyrophosphate extraction, to remove reactive NOM, with mediated electrochemical oxidation (MEO) allowed determining the individual EDC of NOM and Fe<sup>II</sup> in clay minerals. Mediated electrochemical analysis showed systematic differences between samples from two locations in the Netherlands, Zeeland and Limburg. In samples from Zeeland, the reduction potential was higher, the EAC was larger, and the contribution of NOM to the EDC was smaller compared to samples from Limburg. These differences can be attributed to partial oxidation of Boom Clay in Zeeland during its diagenetic history but partial oxidation could also be a storage artefact. The electron yield obtained by pyrite oxidation in samples from Zeeland was larger compared to those from Limburg, which can be explained by a smaller particle size of pyrite in Zeeland. The size of pyrite particles, in turn, can be used as a proxy for the depositional conditions. The electrochemical activity of Fe in clay minerals did not vary systematically between the two locations in the Netherlands. In general, the fraction of electrochemically active Fe in clay minerals increased with the relative content of 2:1 clay minerals. In comparison with samples from the Netherlands, larger fractions of structural Fe in clay minerals were redox-active in samples from Belgium, which had a higher chlorite or glauconite content. This study demonstrates that mediated electrochemical analysis can reveal redox properties of Boom Clay, which might be of relevance for the migration of redox sensitive radionuclides or when assessing the impact of constructing and operating a repository for nuclear waste on the surrounding host rock.

### 1. Introduction

Clay-rich formations deposited in the early Oligocene (33.9–28.1 Ma) in the Netherlands and Belgium have been proposed as potential host rocks for long-term geological disposal of radioactive waste (De

Preter and Lalieux, 2002; Verhoef et al., 2014). According to the Dutch nomenclature, this clay belongs to the Rupel Clay Member of the Rupel Formation which roughly corresponds to the Boom Formation according to the Belgium system (Vis et al., 2016). Despite the inconsistency with the Dutch nomenclature, the samples from the Rupel Clay Member in the

\* Corresponding author.

E-mail address: [alwina.hoving@tno.nl](mailto:alwina.hoving@tno.nl) (A.L. Hoving).

<https://doi.org/10.1016/j.apgeochem.2020.104681>

Received 22 November 2019; Received in revised form 13 June 2020; Accepted 23 June 2020

Available online 11 July 2020

0883-2927/© 2020 Elsevier Ltd. All rights reserved.

Netherlands will be referred to as Boom Clay as it is well known under this name in the context of radioactive waste disposal. In geological disposal concepts, multiple engineered barriers will isolate the waste from the geological surroundings for an extended period of time. Yet, eventually the engineered barriers are expected to degrade. This will expose long-lived radionuclides to the surrounding host rock which acts as an additional barrier to protect the biosphere from radioactive elements released by the radioactive waste (De Preter and Lalieux, 2002).

Some long-lived radionuclides, such as selenium ( $\text{Se}^{79}$ ), technetium ( $\text{Tc}^{99}$ ) and uranium ( $\text{U}^{238}$ ,  $\text{U}^{236}$ ,  $\text{U}^{234}$ ), are redox sensitive (Delécaut, 2004; Schröder et al., 2017). Changes in redox state can alter their environmental properties such as solubility, sorption behavior, bioavailability and toxicity (Van der Perk, 2006). For example, the three listed radionuclides tend to be more mobile in their oxidized state, while in their reduced states they form low-solubility solids and are, as such, less of a threat to the biosphere (Baston et al., 2002; Bruggeman et al., 2007; Cachoir et al., 2003). Predicting the redox state of these radionuclides is therefore essential for the safety assessments of underground repositories since the redox state largely affects their transport and fate. Once released from the engineered barriers, the redox state of the radionuclides will be determined by the redox properties of the surrounding clay formation.

The Boom Clay is considered to be a 'reducing' environment. Its constituents, including pyrite, organic matter, clay minerals and siderite, can retain radionuclides by adsorption and reduction (Badaut et al., 2012; Breynaert et al., 2010; Bruggeman et al., 2007, 2005; Bruggeman and Maes, 2010; Missana et al., 2009; Scheinost and Charlet, 2008). Although the quantities of these redox-active phases in the Belgian and Dutch Boom Clay have been analyzed (Koenen and Griffoen, 2016; Zeelmaekers et al., 2015), there is not much known about their contribution to the redox reactivity of Boom Clay. Particularly, the amount of iron (Fe) in the clay structure accessible to redox reactions, as well as the redox reactivity of organic matter cannot simply be quantified by mineralogical or elemental analyses.

The reduction potential ( $E_H$ ) of the Belgian Boom Clay has been investigated in various studies using (non-mediated) electrochemical measurements and model calculations based on mineral content and pore water composition (e.g. Baeyens et al., 1985; Beaucaire et al., 2000; De Craen et al., 2004). The  $E_H$  is an indicator for the expected direction of possible redox reactions in the sediment. It can be used to assess the thermodynamically most stable redox state of the radionuclide in the sediment. Summarizing the studies on  $E_H$  in Boom Clay, De Craen et al. (2004) concluded that the reduction potential of undisturbed Boom Clay should be lower than  $-270$  mV, but a more detailed study on the redox equilibrium state of Boom Clay and the mechanisms of the controlling redox processes was recommended. Besides the  $E_H$ , the electron donating and accepting capacities (EDC and EAC) are important parameters for characterizing the redox reactivity of Boom Clay. These capacities provide information on the number of electrons per mass of sediment that may be transferred from or to e.g. radionuclides thus indicating the reducing or oxidizing capacity of the sediment.

Here, we apply mediated electrochemical analyses to determine the redox characteristics of Boom Clay from different locations in Belgium and the Netherlands. In order to facilitate the electron exchange between the electrode and the redox-active constituents in Boom Clay, mediated amperometric and potentiometric analyses were used. These measurements utilize a dissolved mediator, which typically undergo fast, one electron transfer between the reduced and the oxidized species with both the sample and the electrode. Mediated electrochemical oxidation and reduction (MEO and MER) have been successfully applied to quantify the EDC and EAC of solid suspensions of clay minerals (e.g. Gorski et al., 2013, 2012a; Hoving et al., 2017), dissolved organic matter (e.g. Aeschbacher et al., 2012, 2011; Klüpfel et al., 2014), Fe (oxyhydr) oxides (Aeppli et al., 2018; Gorski et al., 2016; Klein et al., 2014) and natural sediments (Hoving et al., 2017; Lau et al., 2016, 2015).

MEO and MER measurements give the time evolution of oxidative

and reductive currents that result from sample addition to the electrochemical cell. While the integral of the current response is a direct measure of the number of transferred electrons, the shape of the current curve provides insight into the kinetics of the electron transfer reactions. Based on the difference in reaction kinetics it is possible to separate the electrochemical responses of different redox-active constituents in clay-rich sediments (Hoving et al., 2017). Organic matter and  $\text{Fe}^{II}$  in clay minerals were found to exhibit fast electron transfer kinetics upon MEO and the corresponding EDC can be separated from the EDC of pyrite, which is oxidized at a slower rate. Mediators have also been applied to more accurately determine  $E_H$  values of humic substances, hematite and goethite (Aeschbacher et al., 2011; Gorski et al., 2016; Klüpfel et al., 2014).

In this study we evaluate whether regional variations in sediment deposition or diagenesis are reflected in different redox properties of Boom Clay. We hereby specifically evaluate whether putative, partial oxidation of Boom Clay at one location in Netherlands (Behrends et al., 2016), can be detected by mediated electrochemical analyses. Furthermore, we explore the redox activity of structurally bound Fe in clay minerals and its relationship to regional variations in clay mineralogy. In order to better constrain the redox properties of clay minerals we combine extraction with pyrophosphate solution with MEO to separate the contributions of organic matter and clay minerals to the EDC. This also allows us to determine the redox activity of organic matter in Boom Clay. Eventually we discuss the relevance of the differences in the redox properties of Boom Clay, which were detected by mediated electrochemical analyses, for the disposal of radioactive waste.

## 2. Methods and materials

### 2.1. Sediments

Sediment samples originate from Boom Clay in the Netherlands and Belgium. The clay-rich sediments tend to be more silty in the upper and lower part of the formation and regularly alternating layers of clay-silt, land-derived organic material and carbonates occur throughout the Boom Clay. The thickness of the Boom Clay varies but rarely exceeds 125 m. The depth of the Boom Clay ranges from 0 to 1500 m below the Dutch mainland (De Mulder et al., 2003; Vis et al., 2016; Weerts et al., 2000).

Fresh samples were taken from two different locations in the Netherlands: from a site close to Borssele in the province of Zeeland in the south-west of the Netherlands, and from a drilling near Grubbenvorst in the province of Limburg in the south-east of the Netherlands. The samples from Zeeland (sample codes start with Z) originate from three neighboring wells and were taken at a depth of around 75 m. The samples were drilled as a whole core in a steel casing to prevent oxidation. The core was cut in 2 cm slices in a 95%  $\text{N}_2$ , 5%  $\text{H}_2$  glovebox, and stored in sealed OPA/PE/Al/PE bags (15/15/12/75  $\mu\text{m}$ , Gruber-Folien GmbH & Co. KG). The samples from Limburg (sample codes start with L) are from depths ranging from 530 to 620 m and originate from a geothermal drilling site which was drilled using a rotary drill (Drillmec 300HH). Material from this drilling could only be collected in the form of cuttings. Immediately after being brought to the surface, clumps of clay were sieved out of drilling mud fluid, quickly washed, and transferred into glass jars (Weck) containing  $\text{O}_2$ -absorbing packages (Anaerocult C, Merck). For both sampling locations, every effort has been made to prevent changes in oxidation state due to exposure to atmospheric oxygen. However, it cannot be excluded that samples could have been partially oxidized during the storage of the cores in the steel casings or during the short exposure of the cuttings before being transferred to the glass jars. Further information about the sampling procedure and documentation about possible storage artefacts can be found in Behrends et al. (2016).

Additionally, Boom Clay samples from a drilling in Mol, Belgium were analyzed. Three samples were selected for their divergent contents

of pyrite, siderite and clay minerals. These samples were selected to obtain additional insight into the reactivity of these Boom Clay constituents towards the mediated electrochemical analyses. The separated clay-size fractions (<0.2  $\mu\text{m}$ ) of these samples were also analyzed. Separated clay-size fractions were obtained using the method described in Zeelmaekers (2011). This involves the removal of carbonates, organic matter and Fe-(oxyhydr)oxides by treatments with a mild acetic acid-Na-acetate buffer, hydrogen peroxide, and Na-dithionite, respectively. Subsequently, centrifugation was used for grain-size fractionation. These samples have been characterized by X-ray diffraction (XRD) and X-ray fluorescence (XRF) following the procedures as described in Zeelmaekers et al. (2015). These samples were not stored anoxically and were thus affected by  $\text{O}_2$  oxidation.

## 2.2. Characterization and alteration of the sediments

### 2.2.1. Geochemical characterization

The particle size distribution was measured by laser diffraction using a particle size analyzer (Mastersizer S long bed ver 2.18, Malvern Instruments Ltd.). Aliquots of the samples were suspended in deionized water and treated in an ultrasonic bath for 10 min. Before measuring, 5 ml of peptization solution (0.4 M  $\text{Na}_2\text{CO}_3$  and 9 mM  $\text{Na}_4\text{P}_2\text{O}_7$  decahydrate) was added to about 0.3 g sample.

Total element concentrations were obtained by analyzing the solid samples using total reflection X-ray fluorescence spectroscopy (TXRF, S2 Picofox, Bruker), and by digestion of the samples in a heated mixture of HF,  $\text{HNO}_3$  and  $\text{HClO}_4$ . After evaporation, the residual was dissolved in 1M  $\text{HNO}_3$  and analyzed with inductively coupled plasma atomic emission spectroscopy (ICP-OES, Spectro Arcos) (Reitz et al., 2004). XRD was performed using a D2 PHASER (Bruker, Co-tube and LINXEYE™ detector). Two samples, L9 and L15, were also quantitatively analyzed using XRD by Qmineral, Leuven, Belgium (CuK $\alpha$  X-ray source; Siemens D5000 with a graphite monochromator in Bragg-Brentano configuration). The clay mineralogy was characterized using Rietveld refinement in combination with the PONKCS method (Partial Or No Known Crystal Structures) (Scarlett and Madsen, 2006; Koenen and Griffioen, 2016). Furthermore, scanning electron microscopy (SEM) was performed on epoxy embedded Boom Clay samples.

The total organic carbon and sulfur contents were quantified by infrared detection of  $\text{CO}_2$  and  $\text{SO}_2$  after high temperature combustion (LECO SC632). Inorganic and organic carbon contents were obtained using a CNS elemental analyzer (Fisons NA 1500) by measuring total carbon in the original samples and measuring organic carbon after decalcification. Decalcification was performed by adding 1M HCl to the sediment samples and shaking these suspensions for 12h. The suspensions were centrifuged and supernatants decanted. Subsequently 1M HCl was added again to react for 4h after which the samples were centrifuged and decanted.

Sequential extractions were conducted to quantify different iron and sulfur pools in the samples. The extraction steps of both methods are shown in Table 1. The first extraction was an iron (Fe)-sequential extraction based on Claff et al. (2010). All extracts were analyzed by (ICP-OES). Additionally, extracts from step 1 and step 2 were analyzed for  $\text{Fe}^{\text{II}}$  using the ferrozine colorimetric method (Viollier et al., 2000). The first three steps of the extraction were carried out inside the glovebox, the last three steps outside the glovebox. Sequential sulfur (S)-extraction was conducted using 6M HCl to extract acid volatile sulfur (AVS), methanol for elemental sulfur, and an acidic chromous chloride solution to extract pyrite (Burton et al., 2011, 2008). In step 1 and 3 the released  $\text{H}_2\text{S}$  was trapped in a Zn-acetate solution. To quantify the extracted S, ZnS was dissolved in HCl and a known amount of  $\text{I}_2$  was added which reacts with  $\text{S}^{2-}$ . The remaining  $\text{I}_2$  was quantified by titration with thiosulfate and from these results the reacted  $\text{S}^{2-}$  could be calculated. Sulfur extracted in step 2 of the S-sequential extraction was quantified by a colorimetric method using Na-cyanide and ferric chloride hexahydrate ( $\text{FeCl}_3 \cdot 6\text{H}_2\text{O}$ ) (Bartlett and Skoog, 1954). Both

**Table 1**

Schemes for the sequential extraction of iron and sulfur.

Step	Extractant (duration)	Target phase	Abbreviation
<i>Fe-sequential extraction (adapted from Claff et al., 2010)</i>			
1	1 M $\text{MgCl}_2$ (1h)	Exchangeable fraction and readily soluble salts.	$\text{Fe}^{\text{II}}_{\text{MgCl}_2}/\text{Fe}^{\text{III}}$
2	1 M HCl (4h)	Siderite, Fe-monosulfide and labile Fe-oxides (e.g. ferrihydrite, lepidocrocite).	$\text{MgCl}_2$ $\text{Fe}^{\text{II}}_{\text{HCl}}/$ $\text{Fe}^{\text{III}}_{\text{HCl}}$
3	0.1 M Na-Pyrophosphate, pH 10.4 (16h)	Fe bound to reactive organic matter.	$\text{Fe}_{\text{PP}}$
4	Na-citrate/dithionite solution buffered to a pH 7.5 with $\text{NaHCO}_3$ (CDB) at 75 °C (2 × 10min)	Crystalline Fe-oxides.	$\text{Fe}_{\text{Dith}}$
5	Concentrated $\text{HNO}_3$ (2h)	Pyrite.	$\text{Fe}_{\text{HNO}_3}$
6	Aqua regia	Residual fraction (Al-Silicates)	$\text{Fe}_{\text{res}}$
<i>S-sequential extraction (Burton et al., 2011)</i>			
1	6M HCl (12h)	Acid volatile sulfur	$\text{S}_{\text{AVS}}$
2	Methanol (16h)	Elemental sulfur	$\text{S}^0$
3	500 g/L chromous chloride solution in 32% HCl (48h)	Pyrite	$\text{S}_{\text{Cr}}$

sequential extractions were performed on duplicate samples.

To obtain more information on Fe oxidation state and structural coordination of Fe, samples Z101-14, Z103–22, L2, L15 and L19 were also analyzed by Mössbauer spectroscopy. Transmission  $^{57}\text{Fe}$  Mössbauer spectra were collected at room temperature (300K) and at liquid helium temperature (4.2K) using a  $^{57}\text{Co}$ (Rh) source.  $\alpha\text{-Fe}$  foil was used for velocity calibration. Details on the fitting procedure of the spectra can be found in the supplementary information.

**2.2.1.1. Size fractionated Boom Clay.** Several Boom Clay samples were treated to separate different redox-active constituents. This was done to underpin the interpretation of the current peaks based on mineral standards presented in our previous study (Hoving et al., 2017).

Size fractionation was performed to separate the redox-active clay minerals, which are concentrated in the clay size fraction, and pyrite, which is enriched in the silt fraction. All manipulations of the samples were performed in the glovebox under  $\text{N}_2/\text{H}_2$  (95%/5%) or Ar atmosphere to avoid reaction with atmospheric oxygen. Before size separation the samples were first reacted with 1M HCl for 1 h to remove any amorphous Fe (oxyhydr)oxides. After centrifugation at 2800g the acid was decanted and the tube refilled with  $\text{N}_2$ -purged ultra-pure water (UHQ, 18.2 MOhm cm, Purelab Ultra, Elga). Subsequently, the samples were wet-sieved (mesh size 63  $\mu\text{m}$ ) to separate the sand size fraction from the silt/clay size fractions. Separation of silt- and clay-sized particles was based on gravitation, and carried out by centrifugation. The clay/silt suspensions were centrifuged at 2000 rpm (860 g) for 2 min and the supernatant was decanted and saved. After addition of fresh  $\text{N}_2$ -purged water to the residue, this procedure was repeated. After decanting, fresh  $\text{N}_2$ -purged water was added again to the residue, the sediment was re-suspended and then centrifuged at 1500 rpm (490 g) for 10 min. This last resuspension and centrifugation step was repeated until the supernatant was clear. The supernatants were eventually combined and contained clay particles <2  $\mu\text{m}$ . The silt-sized residue was also resuspended with  $\text{N}_2$ -purged UHQ water before use in the electrochemical analyses.

### 2.2.2. Removing organic matter

Organic matter was removed from four samples using a Na-pyrophosphate solution in order to separate the EDC of natural organic matter (NOM) from the EDC of  $\text{Fe}^{\text{II}}$  in clay minerals. Na-pyrophosphate is a mild extractant that causes significant dissolution of organic matter without producing major alterations of the sediment (Hayes, 2006). Na-pyrophosphate forms complexes with exchangeable

polyvalent cations causing breakdown of cation bridges that are often responsible for maintaining organic matter in a insoluble, flocculated form (Hayes, 2006; Schnitzer and Schuppli, 1989). As extractant, it can therefore be used to isolate organic matter bound to e.g. clay minerals (Wattel-Koekkoek et al., 2001). Boom Clay samples, L15, L19, Z103-22 and Z101-14, were treated with a Na-pyrophosphate solution according to the third step of the Fe sequential extraction. Subsequently these samples were washed three times, by adding N<sub>2</sub>-purged UHQ water followed by centrifugation, before being analyzed by MEO.

### 2.3. Electrochemical characterization of Boom Clay

For the electrochemical characterization, 2 g of Boom Clay was added to 20 mL of 0.1M NaClO<sub>4</sub> to prepare a homogenized stock suspension. The electrochemical cell set-up used to determine the electron donating and accepting capacities followed the same approach as described in Gorski et al. (2012a). The three-electrode set-up was controlled by a potentiostat (CHI1000C, CH Instruments, Austin, TX, USA) and consisted of a reference electrode (3M NaCl Ag/AgCl), a counter electrode consisting of Pt wire, separated from the working electrode compartment by a porous glass frit (all from Bio-Logic, Claix, France) and a working electrode (glassy carbon crucible, HTW Hochtemperatur-Werkstoffe GmbH, Thierhaupten, Germany). The working electrode also functioned as the reaction vessel in which the measurements were performed and which contained the aqueous solution with electrolyte. The electrolyte used in all experiments was 0.1M NaClO<sub>4</sub>, buffered to pH 7.5 by 0.01M MOPS (3-(N-morpholino)propanesulfonic acid). To facilitate the transfer of electrons between solid particles and the working electrode, dissolved one-electron transfer mediators were added to the electrochemical cell. The mediators used here were 2,2'-azino-bis(3-ethylbenzothiazoline-6-sulphonic acid) (ABTS; standard reduction potential E<sub>H</sub><sup>0</sup> = +0.70 V), 4,4'-Bipyridinium-1,1'-bis(2-ethylsulfonate) (Ziv, E<sub>H</sub><sup>0</sup> = -0.38 V) and 1,1'-trimethylene-2,2'-bipyridyl (TQ, E<sub>H</sub><sup>0</sup> = -0.54 V). A more detailed description of these mediators and the mechanism can be found in Gorski et al. (2013, 2012b).

The electron donating capacity (EDC) and electron accepting capacity (EAC) of the various clay sediments were quantified using the following procedure. ABTS was used as a mediator for determining the EDC and Ziv or TQ were used for measuring the EAC. A constant potential was applied to the electrochemical cell: E<sub>H</sub> = +0.61 V vs SHE for MEO and E<sub>H</sub> = -0.4 V or -0.6 V vs SHE, using Ziv or TQ as mediators, respectively, for MER. The applied potentials and the corresponding mediators were selected to cover approximately the stability field of water at the given pH. This implies that the EDC and EAC can be conceived as the maximum capacities under environmental conditions, which are accessible by MEO or MER. Subsequently ~0.2 mL mediator stock solution (0.02 M) was added resulting in a dissolved mediator concentration that was in approximately tenfold excess to the expected electron transfer capacity of the sediment sample. After the mediator had achieved equilibrium at the applied E<sub>H</sub> and the current had returned to background values, a specific volume of suspended sediment was spiked into the cell (0.02 mL–0.1 mL containing 0.001–0.005 g Boom Clay, or 0.0002 g for the separated clay fraction). The oxidative and reductive current peaks, caused by oxidation or reduction of redox-active species in the sediment were continuously monitored. Integration of the current peaks yields the EDC or EAC in moles of electrons per gram of sample, using the following equations.

$$EDC = \frac{1}{F} \frac{\int_{t_1}^{t_2} I_{ox} dt}{m} \quad \text{and} \quad EAC = \frac{1}{F} \frac{\int_{t_1}^{t_2} I_{red} dt}{m} \quad \text{Eq.1}$$

With F being the Faraday constant (96485 s A mol<sup>-1</sup>), t<sub>1</sub> and t<sub>2</sub> (s) the start and end of the current peak, I (A) the current as a function of time and m (g) the mass of sample added to the electrochemical cell. Each sample was analyzed at least three times by repeated addition to the

electrochemical cell.

Hoving et al. (2017) derived an empirical equation to reproduce the time evolution of the oxidative currents for determining the EDC of clay-rich samples (Eq. (2)). Each of the first two terms describes an oxidative peak and the overall curve is the sum of these peaks plus the background value B. It was demonstrated, that the first term can be ascribed to the fast oxidation of structurally bound Fe<sup>II</sup> in clay minerals and oxidation of organic matter. The second term accounts for the slow oxidation of pyrite. Individual integration of the two terms over time t yields the EDC<sub>fast</sub> and EDC<sub>slow</sub>, respectively.

$$I(t) = A_{clay\&NOM} \frac{k_{1, clay\&NOM} t}{k_{1, clay\&NOM} t + 1} e^{-k_2, clay\&NOM t} + A_{pyrite} \frac{k_{1, pyrite} t}{k_{1, pyrite} t + 1} e^{-k_2, pyrite t} + B \quad \text{Eq.2}$$

The two A parameters (Ampere) are used to scale the corresponding oxidative peaks. The k<sub>2</sub>-constants (s<sup>-1</sup>) represent the steepness of the current decrease and the k<sub>1</sub>-constants (s<sup>-1</sup>) describe the initial increase in the oxidative currents. For fitting Eq. (2) to the measured curves, all parameters were optimized. An iteration procedure based on a Levenberg-Marquardt algorithm was used for fitting the variables based on least squares regression. The convergence criterion was reached when the reduced chi-square between two successive iterations was less than the tolerance value of 1E-9. In the fitting procedure, the k-values were constrained to a specific range based on MEO of reference minerals (see Hoving et al., 2017).

### 2.4. Reduction potential of Boom Clay samples

The E<sub>H</sub> measurements were performed with a Pt-ring electrode with integrated reference electrode (Ag/AgCl, Metrohm). To determine the E<sub>H</sub> of the Boom Clay samples the open circuit potential (E<sub>OCP</sub>) was monitored over time (Sander et al., 2015). Here, the potential difference between the working and reference electrode is measured.

Robust mediated E<sub>OCP</sub> measurements are obtained when the concentrations of the mediator in oxidized and reduced form are large enough to induce a sufficient current for polarizing the electrode (Stumm and Morgan, 1996). In a first approach, this is fulfilled when the concentration of oxidized and reduced form of the mediator exceed at least 1% of the total concentration of mediator at the obtained potential. Therefore, the expected E<sub>H</sub> of the sample should be in the range of ±120 mV around the E<sub>H</sub><sup>0</sup> of the mediator at the pH of the suspension (Sander et al., 2015).

A first estimate of the E<sub>H</sub> for choosing the mediator was based on non-mediated E<sub>OCP</sub> measurements for 12h and on thermodynamic equilibrium calculations based on the electrolyte composition and the mineral assemblage in Boom Clay in Zeeland. Resorufin (7-hydroxy-3H-phenoxazin-3-one) and riboflavin 5'-monophosphate were identified as the most suitable mediators. The amount of mediator to add must be large enough to ensure its mediating function while not altering the redox state of the sediment. The amount of mediator added was therefore substantially smaller than the EDC and EAC of the sediment (~2.5% of the EDC plus EAC). The effect of mediator addition was tested on one Boom Clay sample by adding different amounts of mediator (0.01–0.1 mL of 0.001M mediator). We also tested the influence of adding the mediator in the reduced state versus in the oxidized state.

For mediated E<sub>H</sub> measurements 0.1 mL of suspension containing around 0.1 g/mL sediment was added to 4 mL of background electrolyte. The background electrolyte was a synthetic pore water solution mimicking the composition of Boom Clay pore water at the respective locations in the Netherlands. The composition of these solutions can be found in the supplementary information (SI, Table S1) and was based on pore water concentrations reported by Behrends et al. (2016) and Griffioen et al. (2016) for Boom Clay in the Netherlands. After adding the Boom Clay sample, 0.03 mL of 0.001M mediator was added and the

$E_{\text{OCP}}$  was recorded over time. The measured  $E_{\text{OCP}}$  was considered to be stable when the change in potential was less than 5 mV/h.

### 3. Results

#### 3.1. Chemical composition of natural and altered Boom Clay samples

##### 3.1.1. Variability with depth and between locations

Results of chemical analyses of the Boom Clay samples are presented in the supplementary information (SI, Table S2). In the S-extraction, performed on five Boom Clay samples, almost all extractable S was retrieved in the last extraction step targeting pyrite. Dividing the total S contents by Fe extracted in the step targeting pyrite ( $\text{Fe}_{\text{HNO}_3}$ ), resulted in a molar ratio of approximately 2:1 in all samples, indicating that pyrite indeed represented the dominant pool of S in all Boom Clay samples (SI, Fig. S1). Pyrite contents were, on average, higher in samples from Limburg ( $1.83 \pm 0.30$  wt% pyrite) as compared to samples from Zeeland ( $0.98 \pm 0.06$  wt%). Inorganic carbon content followed the same trend with  $0.81 \pm 0.35$  wt% in Limburg and  $0.04 \pm 0.07$  wt% in Zeeland. In contrast,  $\text{Fe}_{\text{Dith}}$  contents, representing crystalline Fe (oxyhydr)oxides, were higher in Boom Clay collected in Zeeland ( $0.108 \pm 0.053$  wt% Fe) compared to those from Limburg ( $0.045 \pm 0.006$  wt% Fe). The aluminium (Al) content, an indicator for the amount of clay minerals in the sample, was slightly higher in the samples from Zeeland with  $5.91 \pm 0.96$  wt% versus  $3.71 \pm 0.42$  wt% in samples from Limburg. The content of residual Fe ( $\text{Fe}_{\text{res}}$ ), which mostly originates from clay minerals, was not significantly different between the two locations. The organic carbon ( $\text{C}_{\text{org}}$ ) contents were similar at both sites except for one sample, L-19, in which  $\text{C}_{\text{org}}$  was more than two times higher than in all other analyzed samples. The geochemical signature showed some trends with depth. At both sampling locations, the contents of Al and  $\text{C}_{\text{org}}$  increased with depth. The pyrite content showed an opposite trend; it increased with depth in the Limburg samples but decreased with depth in Zeeland samples.

Five samples were analyzed by Mössbauer spectroscopy (Table 2 and SI; Fig. S5). The procedure of fitting the Mössbauer spectra and a table with the fitting parameters and results can be found in the supplementary information (SI, Table S5). In general, the largest spectral contribution came from octahedral  $\text{Fe}^{\text{III}}$ . This fraction equaled 73% of total Fe in sample Z101-14, followed by 60% and 57% in samples L-2 and Z103-22, and was lowest in samples L-15 and L-19 with 53% and 48%, respectively. In spectra from samples L-15 and Z103-22 taken at 4.2K, the contribution of octahedral  $\text{Fe}^{\text{III}}$  in Fe-oxides could be identified by a sextuplet of spectral lines caused by the magnetic hyperfine splitting. In both samples, small amounts of Fe-oxides were measured ( $5.5 \pm 0.5\%$  of total Fe). The second largest spectral contribution could be assigned to octahedral  $\text{Fe}^{\text{II}}$  which presents a doublet of spectral lines. The spectra contain multiple doublets. In the 4.2K spectrum one of the octahedral  $\text{Fe}^{\text{II}}$  doublets can be attributed to siderite based on its characteristic magnetic hyperfine field of 17T (Wade et al., 1999). The total  $\text{Fe}^{\text{II}}$

content decreased following the sequence: Z103-22/L-2 (16%) > L-19 (14%) > Z101-14/L-15 (12%). The pyrite contribution was obtained by fixing the isomer shift to the value reported by Ladrière et al. (2009). The relative contents of pyrite ranged between 11 and 25% of all Fe and agreed with the trend in pyrite contents obtained by sequential extraction and elemental analyses. Also, the spectral contribution of siderite and the sum of contributions of  $\text{Fe}^{\text{II}}$  and  $\text{Fe}^{\text{III}}$  bound in clay minerals, were in line with the results obtained from sequential Fe extraction when ascribing  $\text{Fe}^{\text{II}}_{\text{HCl}}$  contents to siderite and  $\text{Fe}_{\text{res}}$  to clay minerals.

Results from XRF and XRD characterization of Boom Clay samples from Mol, Belgium, can be found in the supplementary information (SI, Table S3 and Table S4) and in Fredericx et al., (2018). With respect to the Fe and clay mineralogy, sample BC90 had the highest contents of pyrite (2 wt%) and 2:1 clay minerals (49 wt%). BC115 contained siderite (4 wt%) in addition to pyrite (0.2 wt%) and 2:1 clay minerals (35 wt%). Sample BC130 was selected for its glauconite content (2 wt%). BC130 had the lowest amount of 2:1 clay minerals of the three samples (26 wt%) and contained 0.4 wt% pyrite.

##### 3.1.2. Characterization of fractionated Boom Clay samples

Boom Clay sample L-15 was separated into a clay size-fraction (L-15C) and silt size-fraction (L-15S). The particle size distribution of sample L-15C was: 99 vol% <8  $\mu\text{m}$ , 1 vol% 8–63  $\mu\text{m}$  and 0 vol% >63  $\mu\text{m}$ , demonstrating that L-15C indeed predominantly consisted of clay-sized particles. The Al content, which is a measure for clay minerals, was 9.2 wt%. Based on the average structural formula of 2:1 clay minerals in Boom Clay,  $\text{K}_{0.33}\text{Na}_{0.02}\text{Ca}_{0.15}(\text{Si}_{3.69}\text{Al}_{0.31})(\text{Al}_{1.14}\text{Mg}_{0.38}\text{Fe}_{0.49})\text{O}_{10}(\text{OH})_2$  (Zeelmaekers et al., 2015), 92 wt% of L-15C consisted of clay minerals (assuming all Al in the clay-size fraction was bound in clay minerals). The remaining S content was 0.26 wt% S, which equals 0.49 wt% pyrite. In sample L-15S, 29 vol% of the particles was <8  $\mu\text{m}$ , 69 vol% 8–63  $\mu\text{m}$  and 2 vol% >63  $\mu\text{m}$ . Its Al content was 4.7 wt% of which a part originated from feldspars. The presence of feldspars was evident from XRD analysis (SI, Fig. S3). After correcting for Al related to the approximately 20 wt% feldspars present in L-15S, the remaining content of clay minerals in L-15S was 25 wt%. The S content was 1.75 wt% which equals 3.3 wt% pyrite. Thus, although both size fractions still contained a mixture of pyrite and clay minerals, L-15C was significantly enriched in clay minerals while L-15S was enriched in pyrite. The methodology of clay size separation of the Mol samples was different and resulted in a smaller particle size (<0.2  $\mu\text{m}$ ) and no measurable pyrite. XRD analysis indicated that these samples mainly consisted of illite-smectite (~50 wt%), followed by smectite (~35 wt%), illite (~6 wt%) and kaolinite (~9 wt%). The clay mineral composition was similar for the three samples except that sample BC130 < 0.2 contained more smectite and less interstratified mixed-layered illite-smectite.

The treatment with Na-pyrophosphate removed 6% (Z103-22) and 12% (Z101-14) of the  $\text{C}_{\text{org}}$  content for Zeeland samples and 36% (L-19) and 53% (L-15) of the  $\text{C}_{\text{org}}$  content for the Limburg samples. Thus, the Limburg samples contained more pyrophosphate-extractable organic matter than the Zeeland samples, implying that the largest fraction of organic matter consisted of less redox-active humin in samples from Zeeland.

#### 3.2. Electrochemical characterization of Boom Clay

##### 3.2.1. EDC and EAC of Boom Clay samples

Oxidative and reductive current peaks resulting from mediated electrochemical oxidation and reduction (MEO and MER) of 10 different Boom Clay samples are shown in Fig. 1. MEO of all Boom Clay samples resulted in a rapid current increase followed by a decrease which can be separated in a kinetically fast and a kinetically slower part often visible as a shoulder. The reductive peaks, resulting from MER, were much sharper than the oxidative current peaks. The maximum reductive currents of all samples from Zeeland were larger compared to those of the samples from Limburg. The difference in maximum reductive current

**Table 2**

Fe speciation (% of total Fe) obtained from deconvolution of Mössbauer spectra.

Sample	$\text{Fe}^{\text{II}}$ pyrite	$\text{Fe}^{\text{II}}$ siderite	$\text{Fe}^{\text{II}}$ clay	$\text{Fe}^{\text{III}}$ total	$\text{Fe}^{\text{III}}$ clay	$\text{Fe}^{\text{III}}$ oxides
Z101-14	11	4	12	73		
Z103-22	21 (17) <sup>a</sup>	6 (10)	16 (16)	57	(51)	(6)
L-2	12	12	16	60		
L-15	25 (24)	11 (18)	11 (12)	53	(41)	(5)
L-19	25	13	14	48		

<sup>a</sup> The numbers between brackets are the spectral contributions (%) obtained from measurement at 4.2K. The other numbers resulted from fitting spectra obtained at 300K.

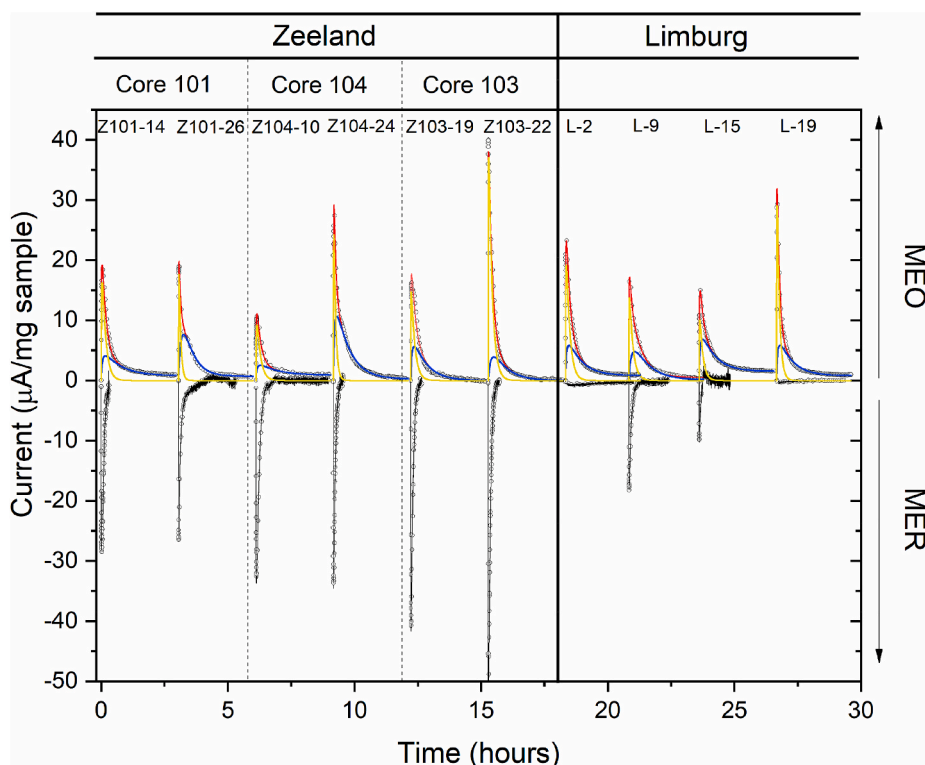


**Fig. 1.** Oxidative (positive) and reductive (negative) current peaks resulting from mediated electrochemical oxidation or reduction of various Boom Clay samples (normalized to 1 mg sample) (open circles). Red lines represent the fitted oxidative peaks using Eq. (2). Beige and blue lines are the isolated current curves obtained from deconvolution of the fitted curve and show the contribution of the EDC with fast (beige) and slow (blue) kinetics. (For interpretation of the references to color in this figure legend, the reader is referred to the Web version of this article.)

was also reflected in the EAC (Table 3); the average EAC of samples from Zeeland of  $61.7 \pm 15.6 \mu\text{mol e}^-/\text{g}$  was larger compared to that of samples from Limburg of  $16.9 \pm 19.3 \mu\text{mol e}^-/\text{g}$ . The EDC was on average  $148.4 \pm 38.5 \mu\text{mol e}^-/\text{g}$  for Zeeland samples which was slightly but not significantly lower than the average EDC obtained for samples from Limburg,  $174.5 \pm 14.8 \mu\text{mol e}^-/\text{g}$ . Fig. 1 also shows the results from fitting to the current curves in order to separate the contribution to the EDC with fast kinetics, representing Fe from clay minerals and NOM,

**Table 3**

Electron donating and accepting capacities (EDC and EAC) obtained by integrating current peaks resulting from mediated electrochemical oxidation/reduction. EDC<sub>fast</sub> and EDC<sub>slow</sub> represent integrated peaks of the fast and slow part of the oxidative current peak obtained by fitting Eq. (2) to the current peak. Errors represent standard deviations of triplicate measurements.

Sample	Depth <i>m</i>	EDC $\mu\text{mol e}^-/\text{g}$	EDC <sub>fast</sub> $\mu\text{mol e}^-/\text{g}$	EDC <sub>slow</sub> $\mu\text{mol e}^-/\text{g}$	EAC $\mu\text{mol e}^-/\text{g}$
Z101-14	72.64	$152 \pm 14$	$57^a$	$104^a$	$56 \pm 20$
Z101-26	72.88	$139 \pm 10$	$28 \pm 5$	$89 \pm 5$	$39 \pm 9$
Z104-10	75.56	$91 \pm 8$	$29 \pm 4$	$30 \pm 2$	$76 \pm 23$
Z104-24	75.76	$194 \pm 55$	$43 \pm 13$	$130 \pm 38$	$52 \pm 10$
Z103-19	79.10	$119 \pm 5$	$39 \pm 3$	$69 \pm 1$	$76 \pm 11$
Z103-22	79.16	$175 \pm 7$	$75 \pm 2$	$99 \pm 5$	$86 \pm 19$
L-2	525	$173 \pm 12$	$37 \pm 9$	$144 \pm 22$	$13 \pm 15$
L-9	570	$148 \pm 10$	$38 \pm 14$	$94 \pm 10$	$45 \pm 10$
L-15	595	$150 \pm 24$	$40 \pm 4$	$127 \pm 5$	$8 \pm 1$
L-15C		$253 \pm 33$	$217 \pm 28$	$37 \pm 5$	–
L-15S		$89 \pm 8$	$17 \pm 1$	$70 \pm 6$	–
L-19	620	$173 \pm 11$	$50 \pm 3$	$76 \pm 1$	$1 \pm 2$
BC90	90	$61 \pm 1$	$25 \pm 0.4$	$42 \pm 1$	119
BC90 < 0.2		$15^a$	$11^a$	$5^a$	$201^a$
BC115	115	$35 \pm 0.3$	$18 \pm 0.2$	$11 \pm 0.1$	$97 \pm 4$
BC115 < 0.2		$7 \pm 6$	$7 \pm 4$	$0 \pm$	$220 \pm 61$
BC130	130	$12 \pm 1$	$6 \pm 0.5$	$6 \pm 0.5$	$118 \pm 59$
BC130 < 0.2		$6 \pm 2$	$3 \pm 1$	$0 \pm 1$	$178 \pm 46$

<sup>a</sup> The result is based on a single measurement. Replicates could not be used due to bad quality of the current signal, or could not be analyzed due to loss of the sample by oxidation during storage in the laboratory preventing repetition of the measurement.

and the EDC with slow kinetics, representing pyrite. The beige and blue curves represent the deconvoluted current peaks corresponding to EDC<sub>fast</sub> and EDC<sub>slow</sub>, respectively.

The calculated values for EDC<sub>fast</sub> and EDC<sub>slow</sub> are listed in Table 3. The EDC<sub>fast</sub> increased with depth for the samples from Limburg. No consistent trend was observed between EDC<sub>fast</sub> and depth for the Zeeland samples. There was no significant difference in EDC<sub>fast</sub> between the two locations. Values for EDC<sub>slow</sub> varied considerably among the samples from Zeeland and the average value did not differ much from that of samples from Limburg. In Limburg, the EDC<sub>slow</sub> decreased with depth.

The current peaks resulting from MEO and MER of the three selected BC samples from Belgium are presented in Fig. 2. These (oxic) samples gave large reductive current peaks upon MER resulting in EAC values between 119 and 148  $\mu\text{mol e}^-/\text{g}$  (Table 3). The EDC values were much smaller than those from the anoxically stored samples from Zeeland and Limburg. Sample BC90, selected for its high pyrite content, gave a broad oxidative current peak upon MEO and resulted in the largest EDC<sub>slow</sub> compared to the other two samples. Samples BC115 and BC130 gave sharper oxidative current peaks compared to BC90, while the peak with sample BC115 was higher compared to that of sample BC130. The obtained EDC<sub>fast</sub>, EDC<sub>slow</sub> and EAC are listed in Table 3.

### 3.2.2. EDC of fractionated Boom Clay samples

The current peaks of the separated size fractions, clay size (L-15C) and silt size (L-15S) of Boom Clay sample L-15, are shown in Fig. 3. L-15C displayed a sharp oxidative current peak upon MEO while addition of L-15S resulted in a broad, low amplitude peak in MEO. The total EDC of the clay-size fraction of  $253 \mu\text{mol e}^-/\text{g}$  was almost three times higher than that of the silt-size fraction with  $89 \mu\text{mol e}^-/\text{g}$ . The EDC<sub>fast</sub> of the clay-size fraction was about 86% of the total EDC, while for the silt-size fraction EDC<sub>fast</sub> only contributed 19% to the total EDC.

MEO of the size separated clay fraction of selected samples from Belgium resulted in much smaller oxidative current peaks compared to the current peak of L-15C. The EDC values were between 4 and 15  $\mu\text{mol e}^-/\text{g}$  representing only 9–30% of the EDC values of the corresponding bulk samples. The clay-size fraction of BC90 resulted in a EDC<sub>slow</sub> of 5

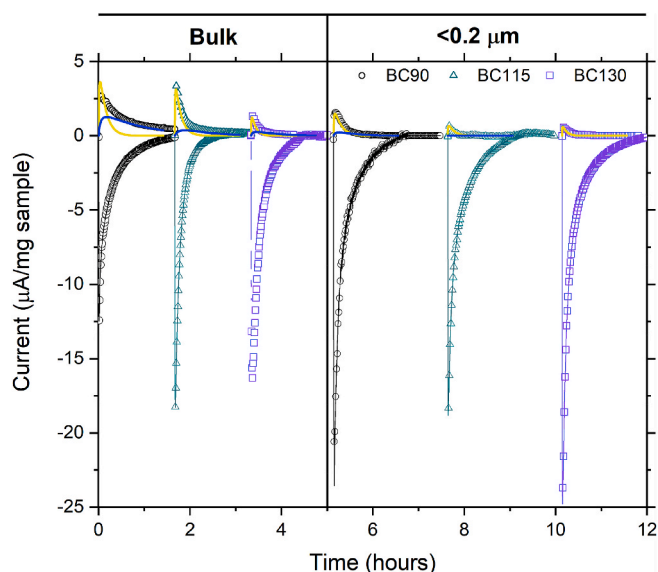


Fig. 2. Oxidative (positive) and reductive (negative) current peaks resulting from mediated electrochemical oxidation or reduction of Boom Clay samples from Mol, Belgium and of the separated clay size fraction of these samples (normalized to 1 mg sample).

$\mu\text{mol e}^-/\text{g}$ , while the clay-size fractions of the other two samples had no detectable  $\text{EDC}_{\text{slow}}$ . MER resulted in higher reductive current peaks compared to the bulk samples. The EAC was around 1.4 to 1.8 times higher compared to the EAC of the bulk samples (Table 3).

The effect of removing natural organic matter (NOM) by pyrophosphate extraction on the oxidative current peaks was only minor (Fig. 3 shows sample L-15 as example). The heights of the current peaks after NOM removal were slightly lower compared to the unaltered samples. After the maximum current had been reached, the current peaks followed virtually the same course. NOM removal resulted in a decrease in  $\text{EDC}_{\text{fast}}$  which was on average  $8 \pm 2.3 \mu\text{mol e}^-/\text{g}$  (~18%) lower for samples from Limburg and  $0.7 \pm 1.1 \mu\text{mol e}^-/\text{g}$  (~1.2%) lower for samples from Zeeland compared to the  $\text{EDC}_{\text{fast}}$  of the unaltered samples. The  $\text{EDC}_{\text{slow}}$  was not significantly affected by NOM removal. After extraction, the EDC of the pyrophosphate solutions was measured. The EDC obtained in these solutions corresponded to the loss in EDC from the Boom Clay samples.

### 3.2.3. Reduction potential

The open circuit potential ( $E_{\text{OCP}}$ ) slowly decreased over time when

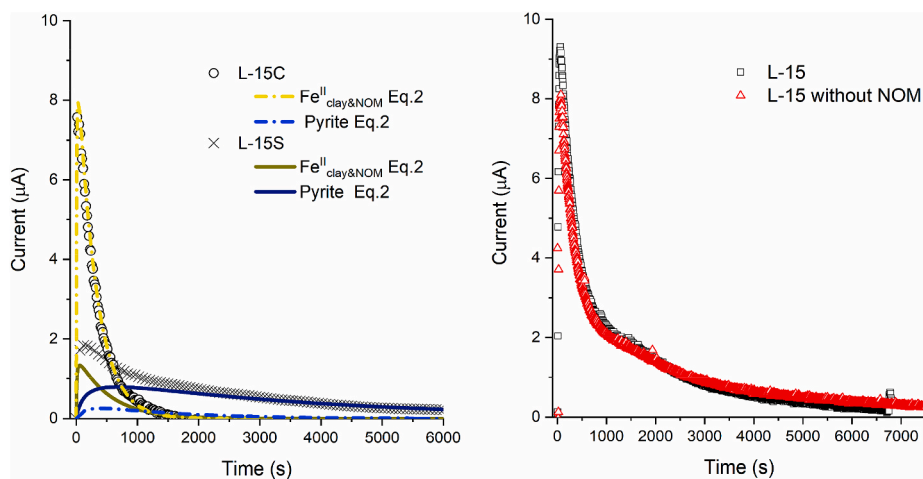


Fig. 3. Left: Oxidative current peaks resulting from mediated electrochemical oxidation of the clay size fraction (0.0001 g) and the silt size fraction (0.0005 g) of sample L-15. Beige and blue lines (dashed and solid) represent deconvoluted current peaks obtained from Eq. (2). Sample quantities were based on the respective clay content and silt content in 1 mg total L-15 sample. Right: Current peaks resulting from mediated electrochemical oxidation of Boom Clay sample L-15 (black squares) and sample L-15 treated with Na-pyrophosphate to remove reactive natural organic matter (NOM) (red triangles). (For interpretation of the references to color in this figure legend, the reader is referred to the Web version of this article.)

Boom Clay material was added to the background electrolyte in the absence of a mediator (Fig. 4). Upon addition of the mediator, a fast change in potential occurred and the  $E_{\text{OCP}}$  stabilized at a constant level. Resorufin appeared to be less suitable as mediator for these samples since the measured potentials reached values below  $-0.2 \text{ V}$  which is outside the  $\pm 0.12 \text{ V}$  range of the standard reduction potential of resorufin ( $-0.03 \text{ V}$ ). Systematically varying the amount of mediator addition between 0.03 and 0.06 mL of 0.001M riboflavin did not have a significant effect on the  $E_{\text{OCP}}$  obtained after stabilization. However, adding very small volumes (0.01 mL) of mediator did not sufficiently increase electron transfer kinetics and therefore the  $E_{\text{OCP}}$  kept drifting after mediator addition. For sample Z101-14, the influence of adding the mediator in reduced form versus oxidized form was tested. The different initial redox state of riboflavin did not result in a different steady state  $E_{\text{OCP}}$  of the sample. Even though only a small subset of Boom Clay samples was used to test mediated potentiometry, a seemingly consistent difference was observed between the  $E_{\text{OCP}}$  of the Zeeland samples and the two Limburg samples (Table 4). The  $E_{\text{OCP}}$  of the samples from Zeeland was on average slightly higher (0.078 V) than the  $E_{\text{OCP}}$  of the samples from Limburg.  $E_{\text{OCP}}$  measurements of pyrite in the synthetic pore water resulted in  $-0.249 \text{ V}$  at pH 7.5.

## 4. Discussion

### 4.1. Redox-activity of Boom Clay constituents

#### 4.1.1. Redox-activity of pyrite

In our previous study, we attributed the  $\text{EDC}_{\text{slow}}$  to the oxidation of pyrite based on measurements of reference materials. However, confirmation of this approach based on the analysis of natural samples has been lacking so far. The validity of the interpretation can be tested by the MEO of separated size fractions of Boom Clay from Limburg, L-15C and L-15S, as the relative enrichment or depletion of pyrite in the two samples should be reflected in the corresponding  $\text{EDC}_{\text{slow}}$ . Indeed, the relative contribution of  $\text{EDC}_{\text{slow}}$  to the total EDC is for L-15C (about 16%) significantly smaller than in L-15S (about 80%), consistent with the depletion of pyrite and increase in the concentration of clay minerals in the clay size fraction. However, when relating the  $\text{EDC}_{\text{slow}}$  to the pyrite contents it becomes evident that oxidation of pyrite is incomplete during MEO as concluded previously (Hoving et al., 2017). For L-15C, MEO resulted in the transfer of about  $1 \mu\text{mol e}^-$  per  $\mu\text{mol}$  pyrite in the sample added. MEO of L-15S on the other hand yielded  $0.25 \mu\text{mol e}^-$  per  $\mu\text{mol}$  pyrite in the sample. The larger electron yield per mol of pyrite for L-15C can be explained by the smaller particle size of pyrite in the clay size fraction. The finding is in accordance with the particle size dependency of pyrite oxidation during MEO, which has been observed and

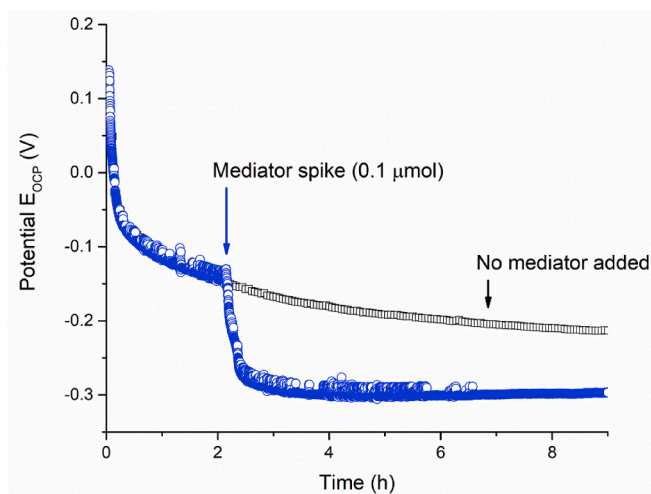


Fig. 4. Open circuit potential ( $E_{\text{OCP}}$ ) measurements of Boom Clay sample Z101-14 over time without and with addition of mediator ( $E_{\text{OCP}}$  as V vs Ag/AgCl sat. KCl. 0 V vs SHE =  $-0.199$  V vs Ag/AgCl sat. KCl).

Table 4

Open circuit potentials ( $E_{\text{OCP}}$ ) of a subset of Boom Clay samples measured by mediated potentiometry using riboflavin as mediator.

Sample	Potential measured in synthetic pore water (V vs SHE)
Z103-22	$-0.186$
Z101-14	$-0.118$
Z104-24	$-0.221$
L15	$-0.241$
L19	$-0.253$
Pyrite (cubic)	$-0.249$

discussed previously (Hoving et al., 2017).

#### 4.1.2. Redox-activity of NOM

In our previous study, the  $\text{EDC}_{\text{fast}}$  was ascribed to the oxidation of Fe (II) in clay minerals and NOM (Hoving et al., 2017). However, no attempts were made to separate the respective contribution of the two constituents as it was estimated that NOM only has a small share of the Boom Clay's EDC. Here, we used pyrophosphate extraction to selectively remove NOM to verify the assumptions and conclusions in Hoving et al. (2017). The pyrophosphate extraction does not completely remove NOM but it can be assumed that it mobilizes the electrochemically active fraction. Quinone and phenolic moieties are generally considered to be the most redox-active fraction of natural organic matter (Aeschbacher et al., 2012, 2011; Walpen et al., 2016). Wattel-Koekkoek et al. (2001) showed that phenolic and alkyl-aromatic compounds were extracted by alkaline and pyrophosphate extractions, leaving behind the less redox-active n-alkanes and n-alkenes. Consequently, the contribution of non-pyrophosphate-extractable NOM to the total EDC is assumed to be negligible.

Our assumption that NOM contributes to  $\text{EDC}_{\text{fast}}$  is confirmed by comparing the oxidative curves before and after pyrophosphate treatment as removal of NOM only decreased the  $\text{EDC}_{\text{fast}}$  but did not affect the  $\text{EDC}_{\text{slow}}$ . Normalizing this decrease in  $\text{EDC}_{\text{fast}}$  to the NOM content extracted by Na-pyrophosphate results in an average  $\text{EDC}_{\text{NOM}}$  of  $1.7 \pm 0.8$  mmol  $e^-$ /g C. This value is in good agreement with the EDC previously reported for dissolved organic matter in Boom Clay pore water obtained by mechanical squeezing of the sediment (i.e., 2.4 mmol  $e^-$ /g C; Hoving et al., 2017). This finding demonstrates that combining MEO measurements with sequential extraction techniques allows determining the EDC of NOM in clay-rich sediments and delineating the individual contributions of Fe<sup>II</sup> in clay minerals and of reduced moieties in NOM to

the overall  $\text{EDC}_{\text{fast}}$ .

#### 4.1.3. Origin of the EAC

The measured EAC values likely reflected reduction of Fe (oxyhydr)oxides or structural Fe<sup>III</sup> in clay minerals. Selected Fe (oxyhydr)oxides (i. e., goethite, ferrihydrite, and hematite) can be completely reduced in MER until a pH of around 7.0 (Aeppli et al., 2018). At higher pH, when the reaction became less exergonic, the reduction of goethite and hematite was incomplete (Aeppli et al., 2018). Incomplete reduction has been ascribed by the authors to the dependency of electron transfer kinetics on  $\Delta_rG$ . That is, the rates became inaccessible for MER when the thermodynamic driving force became too small. Values of  $\Delta_rG$  depend not only on mineral stability and pH but also on the activity of dissolved Fe<sup>2+</sup>. It can be assumed that dissolved Fe<sup>2+</sup> concentrations upon MER of Boom Clay samples were significantly lower than those in the experiments performed by Aeppli et al. (2018) with pure Fe (oxyhydr)oxides. This implies that the  $\Delta_rG$  has very likely not passed the threshold for incomplete reduction in MER measurements of Boom Clay at pH 7.5 and reduction of Fe (oxyhydr)oxides was most likely complete. The possibility of reducing structural Fe<sup>III</sup> in clay minerals during MER has been demonstrated (Gorski et al., 2012a; Hoving et al., 2017). The amount of structural Fe<sup>III</sup> in clay minerals largely exceeds the measured EAC of the Boom Clay samples, implying that not all of this Fe<sup>III</sup> pool was redox-active, which is in agreement to previous findings (Hoving et al., 2017). The amount of Fe (oxyhydr)oxides is negligible in samples from Limburg which coincides with a low EAC. In samples from Zeeland, which contain Fe (oxyhydr)oxides, the average EAC was around four times larger compared to samples from Limburg. Linear regression of EAC vs.  $\text{Fe}_{\text{Dith}}$  (SI, Fig. S7) yields a slope of around 500  $\mu\text{mol } e^-$  (wt%  $\text{Fe}_{\text{Dith}})^{-1}$ . This value is larger than the maximum EAC that can be ascribed to Fe (oxyhydr)oxides (179  $\mu\text{mol } e^-$  (wt% Fe)<sup>-1</sup>). This indicates that Fe (oxyhydr)oxides had considerable contributions to the measured EAC but cannot solely account for the measured EAC. Consequently, despite the fact that Fe<sup>III</sup> in clay minerals was mostly non-reactive in MER, the positive trend between  $\text{Fe}_{\text{Dith}}$  and EAC suggests that reactive Fe<sup>III</sup> in clay minerals increased with  $\text{Fe}_{\text{Dith}}$  content, which, in turn, might reflect the extent of oxidation of the sample during diagenesis or storage.

In contrast to Boom Clay samples from the Netherlands, reduction of Fe<sup>III</sup> in clay minerals was likely the only contribution to the EAC of the  $<0.2$   $\mu\text{m}$  size-fraction of the selected Boom Clay samples from Belgium. The fact that there was no 1 M HCl – extractable Fe<sup>III</sup> in these samples indicated that they did not contain any Fe (oxyhydr)oxides. The  $<0.2$   $\mu\text{m}$  size-fraction from the Belgium Boom Clay has been treated by H<sub>2</sub>O<sub>2</sub> and the samples have been stored under oxic conditions. Most likely, the redox active Fe in the clay minerals of unaltered Boom Clay in Belgium is predominately in the form of Fe<sup>II</sup> similarly to the samples of Limburg and Zeeland. The EAC of the oxidized clay-size samples then reflects Fe<sup>III</sup> in clay minerals which has been produced by oxidation of Fe<sup>II</sup> in clay minerals during treatment and storage.

#### 4.2. Regional differences in redox properties and their relationship to diagenetic history

Boom Clay at the Zeeland location, in contrast to material from the location in Limburg, may have been subjected to partial oxidation either during an event in the sedimentary history or during storage (Behrends et al., 2016). Indications for the oxidation event are low pyrite and carbonate concentrations and the presence of Fe (oxyhydr)oxides. Hence, it can be hypothesized that the partial oxidation is reflected in the redox properties probed by mediated electrochemical analysis. Indeed, systematic differences in the electrochemical properties between samples from Zeeland and Limburg can be ascribed to partial oxidation of Boom Clay in Zeeland:

- (1) The EAC of Zeeland samples was larger compared to that of Limburg, which can be explained by formation of Fe (oxyhydr)

oxides upon partial oxidation of siderite or pyrite or partial oxidation of structurally bound Fe<sup>II</sup> in clay minerals.

- (2) The decrease in EDC<sub>fast</sub> upon NOM removal was larger for samples from Limburg (decrease by 18 ± 3%) compared to those from Zeeland (1.3 ± 2%). The total organic carbon (C<sub>org</sub>) concentrations in samples from Limburg and Zeeland were similar but samples from Limburg contained five times more Napyrophosphate extractable C<sub>org</sub>. Humic and fulvic substances are effectively extracted by alkaline Na-pyrophosphate while a large part of the kerogen will remain (Bein and Sandler, 1983; Fox et al., 2017). Both, reversible oxidation or oxidative degradation of the reactive fulvic and humic acids at the Zeeland site during the oxidation event, can account for different contributions of NOM to EDC<sub>fast</sub>. However, it cannot be excluded that differences in EAC or the NOM contribution to EDC<sub>fast</sub> are relic features caused by regional differences of the deposited material. For example, the source of NOM (terrestrial, marine, reworked) upon deposition may have been different at the location in Limburg compared to that in Zeeland, resulting in a different reactivity of NOM.
- (3) The E<sub>OCP</sub> of samples from Limburg is lower compared to Zeeland suggesting a more reduced state of Boom Clay in Limburg. However, the interpretation of E<sub>OCP</sub> is not straightforward. For heterogeneous reactions, the E<sub>H</sub> of half reactions not only depends on the properties of the solid phase but also on the composition of the solution (Table 5). The most important elements controlling the redox properties of Boom Clay are Fe, S and C. Table 5 lists possible half reactions for the oxidation of relevant reductants in Boom Clay: pyrite, clay-bound Fe<sup>II</sup>, siderite, dissolved Fe<sup>2+</sup>, and NOM. The E<sub>H</sub> of half reactions involving NOM and Fe in clay minerals cannot be readily assessed based on compositional information due to ambiguity of defining a single standard redox potential (clay minerals: Gorski et al., 2012b; Klüpfel et al., 2014). It is very likely that the different possible redox couples in Boom Clay were not in equilibrium with each other. Hence, the measured E<sub>OCP</sub> most likely was a mixed potential (Peiffer et al., 1992 and references therein) which reflects the steady state speciation of the mediator. Its steady state speciation, in turn, depends on the kinetics of the mediator's

oxidation and reduction by the individual redox-active constituents in Boom Clay.

Insight in the kinetics of reactions between Boom Clay constituents and redox mediators were provided by results from MEO and MER. Redox reactions with fast kinetics in MEO and MER are expected to be of larger importance in controlling the E<sub>OCP</sub> values compared to reactions that are kinetically hindered, such as the oxidation of siderite or the reduction of sulfate. In its oxidized state, riboflavin can be readily reduced by pyrite, Fe<sup>II</sup> in clay minerals, and reduced moieties in NOM. In the samples from Zeeland, Fe (oxyhydr)oxides were present and most likely dominated the rates of mediator oxidation. When reaction with pyrite dominates the reduction rates of the mediator, the E<sub>OCP</sub> should approach the E<sub>H</sub> value of half reaction 1 (Table 5). However, the measured E<sub>OCP</sub> varied for the samples from Zeeland with values of 47 mV higher and 21–56 mV lower than the calculated E<sub>H</sub> for reaction 1 (Tables 4 and 5). There are several potential explanations for this discrepancy: 1) the value of the calculated E<sub>H</sub> depends on the thermodynamic stability and stoichiometry of the formed Fe (oxyhydr)oxides (Bonneville et al., 2004) and the corresponding assumptions made for calculating E<sub>H</sub> for reaction 1 might be incorrect, 2) the reduction of the Fe (oxyhydr)oxide is not directly coupled to the formation of pyrite, so that the oxidation of the mediator would be linked to reactions 4 and 5, depending whether siderite is formed or not, 3) reversible redox reaction with Fe in clay minerals and NOM also control the redox state of the mediator and the corresponding E<sub>H</sub> deviates from that of reaction (1).

Despite the constraints in the interpretation, the results demonstrate that electrochemical analyses can be very useful to determine differences in the redox state of Boom Clay samples. Additionally, the electrochemical analyses revealed other regional differences between the samples, which cannot be ascribed to a post-depositional oxidation event but might provide information about depositional conditions. The EDC obtained by MEO of pyrite tends to be larger in samples from Zeeland compared to that in samples of Limburg (Fig. 5). For most samples from Zeeland, roughly 2 μmol e<sup>-</sup> were donated per 1 μmol pyrite in the added sample. This ratio is slightly larger than found in experiments with mechanically ground cubic pyrite of particle size <5 μm (Hoving et al., 2017). SEM images show that pyrite in Zeeland is mostly framboidal (SI, Fig. S2) and the specific surface area of the submicron size pyrite particles is most likely larger than that of the

**Table 5**

Stoichiometry of half reactions of possible importance in Boom Clay and the corresponding Nernst equations for the reduction potentials. On the right, the calculated E<sub>H</sub> values, using the pore water composition of the synthetic Zeeland pore water (pH 7.5), pore water from a piezometer in Boom Clay in Limburg (pH 6.6), and pore water from the formation above the Boom Clay in Zeeland, the Breda Formation (pH 6.3).

Half reaction	E <sub>H</sub> @298 K (V vs SHE)	E <sub>H</sub> in Zeeland porewater (V vs SHE)	E <sub>H</sub> in Limburg porewater (V vs SHE)	E <sub>H</sub> in Breda porewater (V vs SHE)
1 $FeS_2 + 11H_2O \leftrightarrow Fe(OH)_3 + 2SO_4^{2-} + 19H^+ + 15e^-$	$E_H = 0.412 - 0.0749pH + 0.0078 \log(SO_4^{2-})$	-0.165	-0.106	-0.076
2 $FeS_2 + 3H_2O \leftrightarrow Fe(OH)_3 + 2S^0 + 3H^+ + 3e^-$	$E_H = 0.628 - 0.059pH$	0.186	0.236	0.259
3 $FeS_2 + 8H_2O + HCO_3^- \leftrightarrow FeCO_3 + 2SO_4^{2-} + 17H^+ + 14e^-$	$E_H = 0.337 - 0.072pH + 0.0084 \log(SO_4^{2-}) - 0.0042 \log(HCO_3^-)$	-0.212	-0.161	-0.131
4 $FeCO_3 + 3H_2O \leftrightarrow Fe(OH)_3 + HCO_3^- + 2H^+ + e^-$	$E_H = 1.029 + 0.05916 \log(HCO_3^-) - 0.1182pH$	-0.050	0.122	0.153
5 $Fe^{2+} + 3H_2O \leftrightarrow Fe(OH)_3 + 3H^+ + e^-$	$E_H = 1.060 - 0.1773pH - 0.059\log(Fe^{2+})$	-	0.132	0.174
6 $Fe^{II} \text{ clay} \leftrightarrow Fe^{III} \text{ clay} + e^-$	$E_H = E_H^0 - \frac{0.0591}{\beta} \log\left(\frac{Fe^{2+}}{Fe^{3+}}\right)$	-	-	-
7 $NOM_{reduced} \leftrightarrow NOM_{oxidized} + n e^-$	Not known	-	-	-

Reaction 1&2: Guo et al. (2016); Kellsall et al. (1999).

Reaction 3: De Craen et al. (2004).

Reaction 4: Bruno et al. (1992); Silva et al. (2002); Sposito (2008); Wersin et al. (1989).

Reaction 5: Sposito (2008).

Reaction 6: Gorski et al. (2012b). For standard clay minerals E<sub>H</sub><sup>0</sup> and β varied from -0.41 to +0.15 V and 0.16 to 0.30, respectively. These values are unknown for clay minerals in Boom Clay.

Reaction 7: Measured E<sub>H</sub> values of reduced model humic substance compounds ranged from -0.24 to -0.20. (Klüpfel et al., 2014). Unknown for Boom Clay.

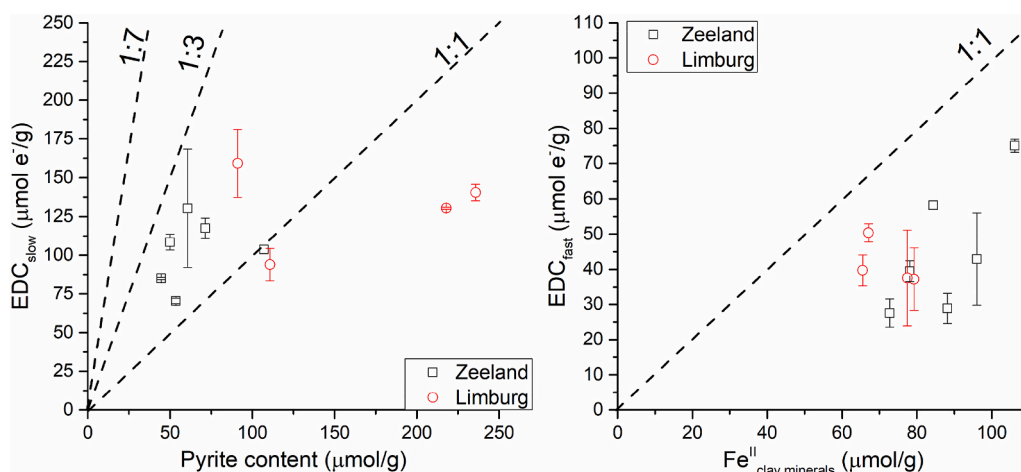


Fig. 5. Left: Electron donating capacity (EDC) of Boom Clay sample constituents that oxidized slowly in mediated electrochemical oxidation (EDC<sub>slow</sub>) plotted versus the pyrite content in those Boom Clay samples. Right: EDC of Boom Clay sample constituents that oxidized rapidly in mediated electrochemical oxidation (EDC<sub>fast</sub>) plotted versus the structural Fe<sup>II</sup> content of clay minerals in the Boom Clay samples. Error bars represent standard deviations of calculated EDC values of triplicate measurements.

mechanically ground hydrothermal pyrite. The effect of surface passivation causing decreased EDC values is expected to be smaller for smaller particles and can explain the relatively high EDC for framboidal pyrite. The other extreme is the low electron yield obtained by oxidizing pyrite of samples L-15 and L-19. In these samples, only about 0.5 μmol e<sup>-</sup> were released per 1.0 μmol pyrite. In these samples, the presence of coarse pyrite particles with a size above 100 μm was observed by SEM imaging (SI, Fig. S2). These particles did not have the typical framboidal shape (SI, Fig. S2). These findings indicate that the ratio between EDC<sub>slow</sub> and pyrite content can be used as an indicator of the particle size distribution of pyrite in the sediments. The size distribution of framboidal pyrite has been proposed as a proxy for the redox conditions during deposition (Wilkin et al., 1996) as framboidal pyrite formed in sediments underlying euxinic bottom waters has a smaller size than that in sediments below oxic or dysoxic bottom waters. The presence of coarse pyrite particles can be explained by euhedral overgrowth of framboidal pyrite (Wilkin et al., 1996) and could be a results of low

sedimentation rates and high rates of pyrite formation.

There is neither a systematic difference in the EDC<sub>fast</sub> nor in the relationship between EDC<sub>fast</sub> and the Fe<sup>II</sup><sub>clay minerals</sub> content (Fig. 5) between samples from Zeeland and Limburg. On average 49 ± 19% of the total Fe<sup>II</sup> in clay minerals in the Limburg and Zeeland samples was accessible by MEO under the given experimental conditions. Thus, not all Fe<sup>II</sup> in clay minerals in Boom Clay was oxidized in MEO and the fraction of redox-active Fe varied among the samples.

However, when including Boom Clay samples from Belgium a systematic trend between the redox activity of structurally bound Fe in clay minerals and the relative content of 2:1 clay minerals emerged. In general, the electron transfer capacity of clay minerals (i.e., ETC<sub>clay</sub>; the sum of EDC<sub>clay</sub> and EAC<sub>clay</sub>) increased with increasing contents of 2:1 clay minerals (Fig. 6). The trendline in Fig. 6 represents this relationship. The measured ETC<sub>clay</sub> of some of the samples were positioned above this trendline implying that the ETC<sub>clay</sub> per % 2:1 clay mineral was higher. This was the case for the samples from Belgium that contained

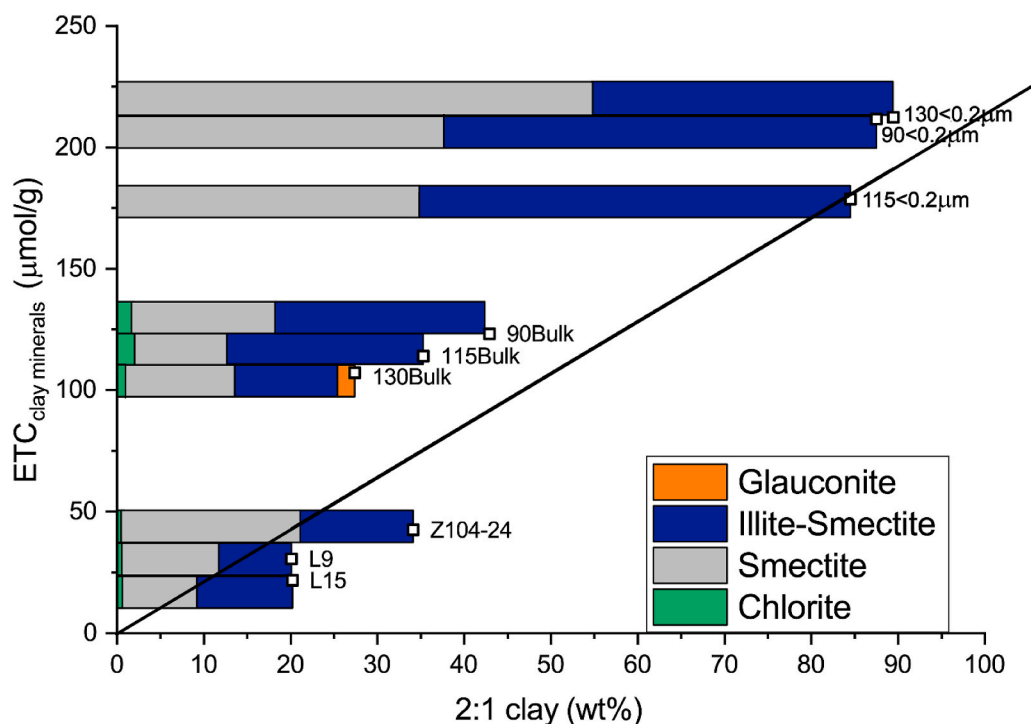


Fig. 6. Electron transfer capacity (ETC) of clay minerals (EDC<sub>clay minerals</sub> + EAC<sub>clay minerals</sub>) in relation to the 2:1 clay mineral content of the samples obtained by XRD analysis. The solid line represents the trendline of the data points.

glaucinite or elevated chlorite contents. In these samples the fraction of redox-active  $\text{Fe}_{\text{clay}}$  ( $\text{ETC}_{\text{clay}}/(\text{Fe}^{\text{II}}_{\text{clay}} + \text{Fe}^{\text{III}}_{\text{clay}})$ ) was between 31 and 41% which was much higher than what was observed in the Dutch samples. Whether Fe was present in smectites or in randomly interstratified mixed-layered illite-smectites did not seem to affect the fraction of redox-active Fe as was observed from the three  $<0.2 \mu\text{m}$  samples from Belgium (24–26%). Gorski et al. (2013) and Neumann et al. (2011a, 2011b) proposed that clay minerals with higher layer charge values are in general less redox-active because a higher layer charge makes it more difficult for the interlayers to expand. Also, the Fe content and its coordination environment in the clay mineral likely influence the susceptibility of Fe to undergo oxidation or reduction. Consequently, regional difference in clay mineral assemblages can imply differences in the redox-activity of structurally bound Fe. Our results demonstrate that the combination of MEO, MER, and sequential extractions allows to probe the redox activity of the clay minerals and to reveal the regional differences.

#### 4.3. Relevance for the disposal of radioactive waste in Boom Clay

Mediated electrochemical analyses indicated regional differences in the redox properties of Boom Clay, which can be attributed to local variations in the deposited material but also different conditions during (early) diagenesis. In the context of the disposal of radioactive waste, particularly the consequences of these differences for the reduction or oxidation of radionuclides by Boom Clay constituents, and the oxidation of Boom Clay during the construction and maintenance of the repository would be of interest.

Comparing the reduction potentials of possible half reactions in Boom Clay with those of radionuclides provides the basis to evaluate whether redox reactions between Boom Clay and redox sensitive radionuclides are exergonic or not. Despite the uncertainties of relating  $E_{\text{OCP}}$  to distinct redox reactions in Boom Clay, the measured value nonetheless is helpful in assessing the reactivity of Boom Clay with radionuclides, assuming that the mediator is a good probe for the redox interactions of radionuclides with Boom Clay. In this case, the measured  $E_{\text{OCP}}$  will provide an indication for the redox speciation of the radionuclide in the host rock. However, further research on relating measured  $E_{\text{OCP}}$  to redox transformations of radionuclides is required to validate the applicability of  $E_{\text{OCP}}$  to predict the redox speciation of radioactive elements in Boom Clay.

Irrespective of the observed regional differences in Boom Clay samples, the theoretical EDC of pyrite exceeds that of other constituents and makes it the potentially most relevant reductant. Our analyses clearly show that MEO, run under the conditions chosen in this work, was poorly suited to quantify the number of electrons that could be donated by pyrite in clay-rich samples; MEO yielded EDC values that were smaller than the theoretically expected EDC of pyrite. At the same time, combining MEO with an independent quantification of pyrite contents – as conducted herein – provides information on the reactivity of the pyrite in the samples. Our findings suggest that the electron yield per mol of pyrite is inversely related to its particle size. Further research is required to assess whether the observed qualitative relationship can be converted into a quantitative relationship. Passivation of the pyrite surface might also affect the reaction with other oxidants than the oxidized mediator, such as the reduction of  $\text{Cr}^{\text{VI}}$  (e.g. Kantar et al., 2015). In this case, the sensitivity of MEO towards surface passivation can be useful in evaluating the redox reactivity of pyrite towards such oxidants, possibly including radionuclides.

The strengths of MEO is to reveal information on the redox properties of NOM and clay minerals in Boom Clay, which is difficult to assess with other techniques. The properties of these components may become relevant when kinetic limitations control redox transformations of radionuclides during migration. This can, for example, be the case when the time scale of reduction by pyrite is longer than the time scale of diffusion and when the reaction of radionuclides with clay minerals or

NOM is faster compared to that of pyrite. Indications for efficient reduction of  $\text{Se}^{\text{IV}}$  by clay minerals have been reported for Boom Clay (Hoving et al., 2017). Also redox-active NOM, and more specifically the quinone moieties, could play an important role in redox transformations of radionuclides. Microbially mediated reduction of  $\text{U}^{\text{VI}}$ , using NOM as an electron shuttle, has been observed (Gu and Chen, 2003). NOM can also reduce radionuclides such as  $\text{Np}^{\text{VI}}$  and  $\text{Pu}^{\text{VI}}$  (Stockdale and Bryan, 2013).

#### Declaration of competing interest

The authors declare that they have no known competing financial interests or personal relationships that could have appeared to influence the work reported in this paper.

#### Acknowledgements

We would like to thank ONDRAF/NIRAS for providing the Boom Clay samples from borehole ON-Mol1, Belgium. The views presented in this paper do not necessarily represent the views of ONDRAF/NIRAS. The research leading to these results has received funding from the Dutch research program on geological disposal OPERA. OPERA is financed by the Dutch Ministry of Economic Affairs and the public limited liability company Elektriciteits-Produktiematschappij Zuid-Nederland (EPZ) and coordinated by the The Central Organization for Radioactive Waste (COVRA).

#### Appendix A. Supplementary data

Supplementary data to this article can be found online at <https://doi.org/10.1016/j.apgeochem.2020.104681>.

#### References

- Aeppli, M., Voegelin, A., Gorski, C.A., Hofstetter, T.B., Sander, M., 2018. Mediated electrochemical reduction of iron (oxyhydr-)oxides under defined thermodynamic boundary conditions. *Environ. Sci. Technol.* 52, 560–570. <https://doi.org/10.1021/acs.est.7b04411>.
- Aeschbacher, M., Graf, C., Schwarzenbach, R.P., Sander, M., 2012. Antioxidant properties of humic substances. *Environ. Sci. Technol.* 46, 4916–4925. <https://doi.org/10.1021/es300039h>.
- Aeschbacher, M., Vergari, D., Schwarzenbach, R.P., Sander, M., 2011. Electrochemical analysis of proton and electron transfer equilibria of the reducible moieties in humic acids. *Environ. Sci. Technol.* 45, 8385–8394. <https://doi.org/10.1021/es201981g>.
- Badaut, V., Schlegel, M.L., Descostes, M., Moutiers, G., 2012. In situ time-resolved X-ray near-edge absorption spectroscopy of selenite reduction by siderite. *Environ. Sci. Technol.* 46, 10820–10826. <https://doi.org/10.1021/es301611e>.
- Baeyens, B., Maes, A., Cremers, A., Henrion, P.N., 1985. In situ physico-chemical characterization of Boom Clay. *Radioact. Waste Manag. Nucl. Fuel Cycle* 6, 391–408.
- Bartlett, J.K., Skoog, D.A., 1954. Colorimetric determination of elemental sulfur in hydrocarbons. *Anal. Chem.* 26, 1008–1011. <https://doi.org/10.1021/ac60090a014>.
- Baston, G.M.N., De Cannière, P., Ilett, D.J., Cowper, M.M., Pilkington, N.J., Tweed, C.J., Wang, L., Williams, S.J., 2002. Technetium behaviour in Boom Clay – a laboratory and field study. *Radiochim. Acta* 90, 735–740. <https://doi.org/10.1524/ract.2002.90.9-11.2002.735>.
- Beaucaire, C., Pitsch, H., Toulhoat, P., Motellier, S., Louvat, D., 2000. Regional fluid characterisation and modelling of water-rock equilibria in the Boom clay Formation and in the Rupelian aquifer at Mol, Belgium. *Appl. Geochem.* 15, 667–686.
- Behrends, T., van der Veen, I., Hoving, A., Griffioen, J., 2016. First assessment of the pore water composition of Rupel Clay in The Netherlands and the characterisation of its reactive solids. *Neth. J. Geosci.* 95, 315–335. <https://doi.org/10.1017/njg.2016.23>.
- Bein, A., Sandler, A., 1983. Early diagenetic oxidation and maturation trends in organic matter extracted from eocene chalks and cherts. *Chem. Geol.* 38, 213–224.
- Bonneville, S., Van Cappellen, P., Behrends, T., 2004. Microbial reduction of iron(III) oxyhydroxides: effects of mineral solubility and availability. *Chem. Geol.* 212, 255–268. <https://doi.org/10.1016/j.chemgeo.2004.08.015>.
- Breyneert, E., Scheinost, A.C., Dom, D., Rossberg, A., Vancluysen, J., Gobechiya, E., Kirschhock, C.E.A., Maes, A., 2010. Reduction of Se(IV) in boom clay: XAS solid phase speciation. *Environ. Sci. Technol.* 44, 6649–6655. <https://doi.org/10.1021/es100569e>.
- Bruggeman, C., Maes, A., Vancluysen, J., Vandemussele, P., 2005. Selenite reduction in Boom clay: effect of FeS<sub>2</sub>, clay minerals and dissolved organic matter. *Environ. Pollut.* 137, 209–221. <https://doi.org/10.1016/j.envpol.2005.02.010>.
- Bruggeman, C., Maes, A., Vancluysen, J., 2007. The interaction of dissolved Boom Clay and Gorleben humic substances with selenium oxyanions (selenite and selenate).

- Appl. Geochem. 22, 1371–1379. <https://doi.org/10.1016/j.apgeochem.2007.03.027>.
- Bruggeman, C., Maes, N., 2010. Uptake of uranium(VI) by pyrite under boom clay conditions: influence of dissolved organic carbon. *Environ. Sci. Technol.* 44, 4210–4216. <https://doi.org/10.1021/es100919p>.
- Bruno, J., Wersin, P., Stumm, W., 1992. On the influence of carbonate in mineral dissolution: II. The solubility of FeCO<sub>3</sub>(s) at 25°C and 1 atm total pressure. *Geochem. Cosmochim. Acta* 56, 1149–1155. [https://doi.org/10.1016/0016-7037\(92\)90052-K](https://doi.org/10.1016/0016-7037(92)90052-K).
- Burton, E.D., Bush, R.T., Johnston, S.G., Sullivan, L.A., Keene, A.F., 2011. Sulfur biogeochemical cycling and novel Fe-S mineralization pathways in a tidally flooded wetland. *Geochem. Cosmochim. Acta* 75, 3434–3451. <https://doi.org/10.1016/j.gca.2011.03.020>.
- Burton, E.D., Sullivan, L.A., Bush, R.T., Johnston, S.G., Keene, A.F., 2008. A simple and inexpensive chromium-reducible sulfur method for acid-sulfate soils. *Appl. Geochem.* 23, 2759–2766. <https://doi.org/10.1016/j.apgeochem.2008.07.007>.
- Cachoir, C., Lemmens, K., Van den Berghe, S., Van Iseghem, P., 2003. UO<sub>2</sub> dissolution in Boom Clay conditions. *J. Nucl. Mater.* 321, 49–59. [https://doi.org/10.1016/S0022-3115\(03\)00199-5](https://doi.org/10.1016/S0022-3115(03)00199-5).
- Claff, S.R., Sullivan, L.A., Burton, E.D., Bush, R.T., 2010. A sequential extraction procedure for acid sulfate soils: partitioning of iron. *Geoderma* 155, 224–230. <https://doi.org/10.1016/j.geoderma.2009.12.002>.
- De Craen, M., Wang, L., Van Geet, M., Moors, H., 2004. Geochemistry of Boom Clay Pore Water at the Mol Site - Status 2004 - Scientific Report BLG-990. Mol, Belgium.
- De Mulder, E.F.J., Geluk, M.C., Ritsema, I.L., Westerhoff, W.E., Wong, T.E., 2003. Dikte van de Rupel klei op het vaste land van Nederland. In: *De Ondergrond Van Nederland*. Noordhoff Uitgevers bv Groningen/Houten, The Netherlands, p. 291, 1–379.
- De Preter, P., Lalieux, P., 2002. Assessing Long-Term Safety of Deep Disposal in Belgium: the SAFIR 2-Report. ONDRAF/NIRAS.
- Delécaut, G., 2004. The Geochemical Behaviour of Uranium in the Boom Clay. PhD Dissertation. Katholieke Universiteit Leuven, Louvain-La-Neuve Belgium.
- Fox, P.M., Nico, P.S., T'faily, M.M., Heckman, K., Davis, J.A., 2017. Characterization of natural organic matter in low-carbon sediments: extraction and analytical approaches. *Org. Geochem.* 114, 12–22. <https://doi.org/10.1016/j.orggeochem.2017.08.009>.
- Frederickx, L., Honty, M., Craen, M.D., Dohrmann, R., Elsen, J., 2018. Relating the cation exchange properties of the boom clay (Belgium) to mineralogy and pore-water chemistry. *Clay Clay Miner.* 66 (5), 449–465.
- Gorski, C.A., Edwards, R., Sander, M., Hofstetter, T.B., Stewart, S.M., 2016. Thermodynamic characterization of iron oxide–aqueous Fe<sup>2+</sup> redox couples. *Environ. Sci. Technol.* 50, 8538–8547. <https://doi.org/10.1021/acs.est.6b02661>.
- Gorski, C. a, Aeschbacher, M., Soltermann, D., Voegelin, A., Baeyens, B., Marques Fernandes, M., Hofstetter, T.B., Sander, M., 2012a. Redox properties of structural Fe in clay minerals. 1. Electrochemical quantification of electron-donating and -accepting capacities of smectites. *Environ. Sci. Technol.* 46, 9360–9368. <https://doi.org/10.1021/es3020138>.
- Gorski, C. a, Klüpfel, L., Voegelin, A., Sander, M., Hofstetter, T.B., 2012b. Redox properties of structural Fe in clay minerals. 2. Electrochemical and spectroscopic characterization of electron transfer irreversibility in ferruginous smectite, SWa-1. *Environ. Sci. Technol.* 46, 9369–9377. <https://doi.org/10.1021/es302014u>.
- Gorski, C. a, Klüpfel, L.E., Voegelin, A., Sander, M., Hofstetter, T.B., 2013. Redox properties of structural Fe in clay minerals: 3. Relationships between smectite redox and structural properties. *Environ. Sci. Technol.* 47, 13477–13485. <https://doi.org/10.1021/es403824x>.
- Griffioen, J., Verweij, H., Stuurman, R., 2016. The composition of groundwater in Palaeogene and older formations in The Netherlands. A synthesis. *Geol. en Mijnbouw/Netherlands J. Geosci.* 95, 349–372. <https://doi.org/10.1017/njg.2016.19>.
- Gu, B., Chen, J., 2003. Enhanced microbial reduction of Cr(VI) and U(VI) by different natural organic matter fractions. *Geochem. Cosmochim. Acta* 67, 3575–3582. [https://doi.org/10.1016/S0016-7037\(03\)00162-5](https://doi.org/10.1016/S0016-7037(03)00162-5).
- Guo, B., Peng, Y., Parker, G., 2016. Electrochemical and spectroscopic studies of pyrite-cyanide interactions in relation to the depression of pyrite flotation. *Miner. Eng.* 92, 78–85. <https://doi.org/10.1016/j.mineng.2016.03.003>.
- Hayes, M.H.B., 2006. Solvent systems for the isolation of organic components from soils. *Soil Sci. Soc. Am. J.* 70, 986. <https://doi.org/10.2136/sssaj2005.0107>.
- Hoving, A.L., Sander, M., Bruggeman, C., Behrens, T., 2017. Redox properties of clay-rich sediments as assessed by mediated electrochemical analysis: separating pyrite, siderite and structural Fe in clay minerals. *Chem. Geol.* 457, 149–161. <https://doi.org/10.1016/j.chemgeo.2017.03.022>.
- Kantar, C., Ari, C., Keskin, S., 2015. Comparison of different chelating agents to enhance reductive Cr(VI) removal by pyrite treatment procedure. *Water Res.* 76, 66–75. <https://doi.org/10.1016/j.watres.2015.02.058>.
- Kelsall, G.H., Yin, Q., Vaughan, D.J., England, K.E.R., Brandon, N.P., 1999. Electrochemical oxidation of pyrite (FeS<sub>2</sub>) in aqueous electrolytes. *J. Electroanal. Chem.* 471, 116–125.
- Klein, A.R., Silvester, E., Hogan, C.F., 2014. Mediated electron transfer from FeII adsorbed onto hydrous ferric oxide and a working electrode. *Environ. Sci. Technol.* 48, 10835–10842.
- Klüpfel, L., Piepenbrock, A., Kappler, A., Sander, M., 2014. Humic substances as fully regenerable electron acceptors in recurrently anoxic environments. *Nat. Geosci.* 7, 195–200. <https://doi.org/10.1038/NNGEO2084>.
- Koenen, M., Griffioen, J., 2016. Characterisation of the geochemical heterogeneity of the Rupel clay member in The Netherlands. *Neth. J. Geosci.* 95, 269–281. <https://doi.org/10.1017/njg.2016.6>.
- Ladrière, J., Dussart, F., Dabi, J., Haulotte, O., Verhaeghe, S., Regout, J., 2009. Mossbauer study of the Boom clay, a geological formation for the storage of radioactive wastes in Belgium. In: *Hyperfine Interactions*. Springer Berlin Heidelberg, pp. 1–9. <https://doi.org/10.1007/s10751-009-9977-9>.
- Lau, M.P., Sander, M., Gelbrecht, J., Hupfer, M., 2016. Spatiotemporal redox dynamics in a freshwater lake sediment under alternating oxygen availabilities: combined analyses of dissolved and particulate electron acceptors. *Environ. Chem.* 13, 826–837. <https://doi.org/10.1071/EN15217>.
- Lau, M.P., Sander, M., Gelbrecht, J., Hupfer, M., 2015. Solid phases as important electron acceptors in freshwater organic sediments. *Biogeochemistry* 123, 49–61. <https://doi.org/10.1007/s10533-014-0052-5>.
- Missana, T., Alonso, U., García-Gutiérrez, M., 2009. Experimental study and modelling of selenite sorption onto illite and smectite clays. *J. Colloid Interface Sci.* 334, 132–138. <https://doi.org/10.1016/j.jcis.2009.02.059>.
- Neumann, A., Petit, S., Hofstetter, T.B., 2011a. Evaluation of redox-active iron sites in smectites using middle and near infrared spectroscopy. *Geochem. Cosmochim. Acta* 75, 2336–2355. <https://doi.org/10.1016/j.gca.2011.02.009>.
- Neumann, A., Sander, M., Hofstetter, T.B., 2011b. Redox properties of structural Fe in smectite clay minerals. In: *Tratnyek, P., et al. (Eds.), Aquatic Redox Chemistry*. American Chemical Society, Washington, DC, pp. 361–379. ACS Symposium Series.
- Peiffer, S., Klemm, O., Pecher, K., Hollerung, R., 1992. Redox measurements in aqueous solutions—a theoretical approach to data interpretation, based on electrode kinetics. *J. cont.hydrol.* 10, 1–18.
- Reitz, A., Pfeifer, K., De Lange, G.J., Klump, J., 2004. Biogenic barium and the detrital Ba/Al ratio: a comparison of their direct and indirect determination. *Mar. Geol.* 204, 289–300. [https://doi.org/10.1016/S0025-3227\(04\)00004-0](https://doi.org/10.1016/S0025-3227(04)00004-0).
- Sander, M., Hofstetter, T.B., Gorski, C.A., 2015. Electrochemical analyses of redox-active iron minerals: a review of nonmediated and mediated approaches. *Environ. Sci. Technol.* 49, 5862–5878. <https://doi.org/10.1021/acs.est.5b00006>.
- Scarlett, N.V.V., Madsen, I.C., 2006. Quantification of phases with partial or no known crystal structures. *Powder Diffr.* 21, 278–284. <https://doi.org/10.1154/1.2362855>.
- Scheinost, A.C., Charlet, L., 2008. Selenite reduction by mackinawite, magnetite and siderite: XAS characterization of nanosized redox products. *Environ. Sci. Technol.* 42, 1984–9.
- Schnitzer, M., Schuppli, P., 1989. Method for the sequential extraction of organic matter from soils and soil fractions. *Soil Sci. Soc. Am. J.* 53, 1418–1424. <https://doi.org/10.2136/sssaj1989.03615995005300050019x>.
- Schröder, T.J., Rosca-Bocancea, E., Hart, J., 2017. Safety Assessment of Uranium on Very Long Timescales - OPERA-PU-NRG733/745.
- Silva, C.A.R., Liu, X., Millero, F.J., 2002. Solubility of siderite (FeCO<sub>3</sub>) in NaCl solutions. *CEUR Workshop Proc* 31, 97–108. <https://doi.org/10.1023/A>.
- Sposito, G., 2008. *The Chemistry of Soils*, Second. Oxford University Press Inc, New York, USA.
- Stockdale, A., Bryan, N.D., 2013. The influence of natural organic matter on radionuclide mobility under conditions relevant to cementitious disposal of radioactive wastes: a review of direct evidence. *Earth Sci. Rev.* 121, 1–17. <https://doi.org/10.1016/j.earscirev.2013.02.007>.
- Stumm, W., Morgan, J.J., 1996. *Aquatic Chemistry: Chemical Equilibria and Rates in Natural Waters*, third ed. Wiley-Interscience, New York.
- Van der Perk, M., 2006. *Soil and Water Contamination, from Molecular to Catchment Scale*. Taylor and Francis Ltd.
- Verhoef, E., Neef, E., Grupa, J., Poley, A., 2014. Outline of a disposal concept in clay. OPERA-PG-COV008.
- Viollier, E., Inglett, P.W., Hunter, K., Roychoudhury, A.N., Van Capelle, P., 2000. The ferrozine method revisited: Fe(II)/Fe(III) determination in natural waters. *Appl. Geochem.* 15, 785–790.
- Vis, G.J., Verweij, H., Koenen, M., 2016. The Rupel Clay Member in The Netherlands: towards a comprehensive understanding of its geometry and depositional environment. *Geol. en Mijnbouw/Netherlands J. Geosci.* 95, 221–251. <https://doi.org/10.1017/njg.2016.25>.
- Wade, M.L., Agresti, D.G., Wdowiak, T.J., Armendarez, L.P., Farmer, J.D., 1999. A Mössbauer investigation of iron-rich terrestrial hydrothermal vent systems: lessons for Mars exploration. *J. Geophys. Res. Planets* 104, 8489–8517.
- Walpen, N., Schroth, M.H., Sander, M., 2016. Quantification of phenolic antioxidant moieties in dissolved organic matter by flow-injection analysis with electrochemical detection. *Environ. Sci. Technol.* 50, 6423–6432. <https://doi.org/10.1021/acs.est.6b01120>.
- Wattel-Koekoek, E.J.W., Van Genuchten, P.P.L., Buurman, P., Van Lagen, B., 2001. Amount and composition of clay-associated soil organic matter in a range of kaolinitic and smectitic soils. *Geoderma* 99, 27–49. [https://doi.org/10.1016/S0016-7061\(00\)00062-8](https://doi.org/10.1016/S0016-7061(00)00062-8).
- Weerts, H.J.T., Cleveringa, P., Ebbing, J.H.J., De Lang, F.D., Westerhoff, W.E., 2000. *De lithostratigrafische indeling van Nederland – Formaties uit het Tertiair en Kwartair*.
- Wersin, P., Charlet, L., Karthein, R., Stumm, W., 1989. From adsorption to precipitation: sorption of Mn<sup>2+</sup> on FeCO<sub>3</sub>(s). *Geochem. Cosmochim. Acta* 53, 2787–2796. [https://doi.org/10.1016/0016-7037\(89\)90156-7](https://doi.org/10.1016/0016-7037(89)90156-7).
- Wilkin, R.T., Barnes, H.L., Brantley, S.L., 1996. The size distribution of framboidal pyrite in modern sediments: an indicator of redox conditions. *Geochem. Cosmochim. Acta* 60 (20), 3897–3912.
- Zeelmaekers, E., 2011. *Computerized Qualitative and Quantitative Clay Mineralogy: Introduction and Application to Known Geological Cases*. Katholieke Universiteit Leuven.
- Zeelmaekers, E., Honty, M., Derkowski, A., Śródoń, J., De Craen, M., Vandenberghe, N., Adriaens, R., Ufer, K., Wouters, L., 2015. Qualitative and quantitative mineralogical composition of the rupelian boom clay in Belgium. *Clay Miner.* 50, 249–272. <https://doi.org/10.1180/claymin.2015.050.2.08>.